Modelling of Air Pumping Noise and Study of Tread Pattern Pitch

Ting-Wei Guo[1*] and Jung-Ho Cheng[1]

[1] Department of Mechanical Engineering, National Taiwan University, No. 1, Sec. 4, Roosevelt Rd., Taipei City 10617, Taiwan R.O.C.
[*] Corresponding author. E-mail: r01522509@ntu.edu.tw

Received: Aug. 16, 2020; Accepted: Oct. 05, 2020

The sources of noise from a pneumatic tire are complex. They include the vibrations of the tread block and carcass, tread block slip friction, carcass inner standing wave patterns and air pumping of the tread pattern. The frequency of the air pumping of the tread pattern ranges from 800 to 1200 Hz, which is the typical frequency range to which human ears are sensitive. Therefore, air pumping has a direct influence on noise. This study uses the finite element software, Abaqus, and the fluid mechanics software, FlowVision, to establish an air pumping noise model for tires. The model simulates the air pumping effects of the tire tread. The change in sound pressure is converted from the time domain to the frequency domain by fast Fourier transforms, and A-weighting modified sound pressure levels are added to calculate the spectrum and the total sound pressure level. The air pumping noise model for tires was verified experimentally and utilized to study the influence of tread pattern pitch on the air pumping noise.

Keywords: radial tire, air pumping, tread pattern noise, fluid structure coupling

http://dx.doi.org/10.6180/jase.202104_24(2).0004

1. Introduction

In the past, the tire industry was typically concerned with the performance of grip, handling, wear, and durability. However, the appeal for environmental protection and quality of life demands attention to the noise problems of tires. Table 1 presents the noise standards for Class C1 tires set forth by the EU [1]. The second stage of these standards was implemented in November 2016. If the performance of a tire does not pass the standards, it is forbidden to it sell in the EU region. This regulation will become more stringent and become the technical threshold for tire manufacturing, now and in the future.

Fig. 1 illustrates the sources of noise [2, 3], which can be divided into two categories: tread pattern and carcass noise. Each noise has its own mechanism and frequency range, and the mechanisms are coupled with one another. If all mechanisms are proposed simultaneously, the model is difficult to build, and the computational time is too long. Hence, most noise research studies only one mechanism at a time. For example, T. Sakata [4], and H.M.R Aboutorabi [5] studied the carcass inner standing wave and vibration by vehicle test data and modal analysis. S. Fujiwara [6] used basic formulas to predict the influence of adding different forms of tread patterns beside the groove on noise. Then the acoustic software and experimental data were utilized to verify the results and study noise reduction. M.-X. Huang [2] used spectra obtained from experiments to understand the mechanisms of noise at different frequencies for slicks, groove, and complete tread patterns. Y. Wei [7] combined Lagrangian and Eulerian functions to simulate the vibrations of the tread block, where simulation results were similar to the experimental data. From M.-X. Huang's research [2, 8], we know the noise of frequency in the range of 800-1200 Hz is the main source. The noise mechanism of this frequency range is air pumping and vibration of the tread block. This study focuses on the air pumping noise and establishes a predictive model.

Outdoor vehicle and indoor tests are generally used to measure noise. Although the outdoor vehicle test is a formal noise test, it is difficult to prepare for the environment and have adequate space. The indoor test is easier to prepare and control the environment factors. Therefore, this study builds the air pumping noise model for tires

Table 1. EU standard for stage and grade of tire noise performance for Class C1 tires [1].

Stage 1		Stage 2	
Nominal section width	Limit dB(A)	Nominal section width	Limit dB(A)
145 and lower	72	185 and lower	70
Over 145 up to 165	73	Over 185 up to 245	71
Over 165 up to 185	74	Over 245 up to 275	72
Over 185 up to 215	75	Over 275	74
Over 215	76		

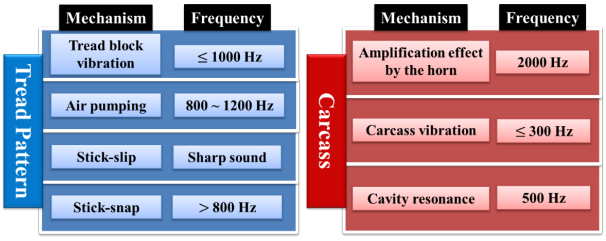

Fig. 1. Noise mechanisms of tire and frequency range [2,3].

according to the indoor test and refers to Y.-H. Huang's method [3] that used two software programs to simulate fluid structure coupling analysis. Finally, the simulation results were verified experimentally, and the tread pattern pitch was studied further.

2. Air Pumping Noise Model for Tires

The deformation of a tire and the change of flow field need to be considered when simulating the noise during tire rolling. Finite element software, Abaqus, is able to simulate the deformation of tires and contact problems between the bead, rim, tread and ground. Fluid mechanics software, FlowVision, simulates the change in the flow field. Fig. 2 depicts how to use Abaqus and FlowVision to establish the model and fluid structure coupling. Fig. 3 depicts how FlowVision's Multi-Physics Manager connects with Abaqus to control the exchange of data [9]. After FlowVision calculates an increment, the pressure exerted by the fluid on the tire surface is transferred to Abaqus. Abaqus calculates the deformation of tire with this pressure reading. When the increment of Abaqus reaches the same amount as the previous transfer of FlowVision, Abaqus outputs the data of deformation of the tire that are the node coordinates of each element. This data was utilized by FlowVision as a geometric boundary to calculate the change of fluid field. Finally, the results of the fluid structure coupling analysis were outputs for the noise analysis. The modeling of Abaqus and FlowVision is described in the next sections.

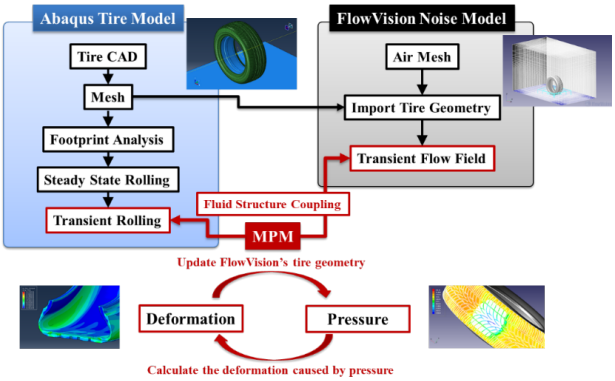

Fig. 2. Fluid structure coupling process of Abaqus and FlowVision.

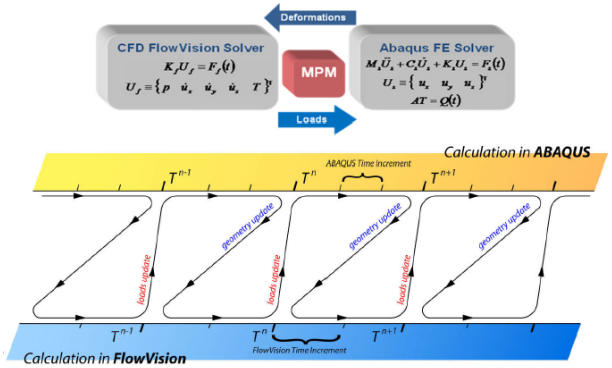

Fig. 3. Control increment and exchange data [9].

2.1. Abaqus Tire Model

A 205/55R16 91 V tire was modeled for this study. To reduce complexity and computational time, we introduced the following assumptions concerning the tire model:

1. Rubber is isotropic and homogeneous with a Poisson's ratio of 0.475.
2. The drum of the indoor test is changed to a flat surface.
3. The flat surface and rim are rigid.
4. The coefficient of friction between the tread and flat surface is 0.7.

5. The influence of the temperature on rubber and air is not taken into account.

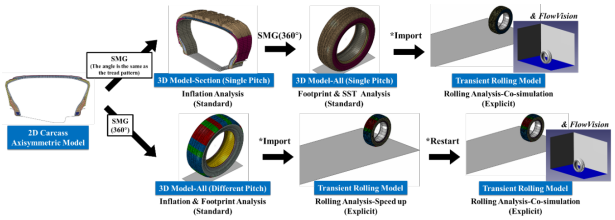

Fig. 4. The modeling process of tire model of Abaqus.

Fig. 4 illustrates the modeling process of the tire model. The 2-D axisymmetric model of the carcass was built, and the parts of rubber and bead wire used the continuum elements, CGAX4 and CGAX3. The belt, cover, and ply were defined by rebar, and the elements SFMGAX1 were used. The commands of finite element software Abaqus are used in the modeling process, and these commands are marked by a *. *Symmetric Model Generation was used to convert the 2-D model to a 3-D model while the tread pattern was added to the model. The surfaces of the tread pattern and carcass were defined by *Tie.

The 3-D modeling process is different depending on the pitch arrangement. If we study a single pitch, the 2-D carcass model is converted to a 3-D section model and adds the section tread pattern on the carcass. Then simulating the inflation analysis, *Symmetric Model Generation and *Symmetric Results Transfer were used to build the whole tire model and simulate the footprint analysis. The pitch length of each tread pattern in the circumferential direction was the same. Finally, *Steady State Transport was utilized to simulate steady state rolling, and the result of steady state rolling was used as the initial condition by *Import for fluid structure coupling analyses. If the full set of pitch arrangements were studied, the 2-D carcass model can be directly converted to the 3-D whole tire model. Then the all-tread pattern of different pitch arrangements was added to the 3-D model to simulate the footprint analysis. Because *Steady State Transport cannot be used, Abaqus/Explicit was used to simulate tire rolling. The result of the footprint analysis was taken as the initial condition by *Import to simulate tire rolling until the velocity was stable, and then the fluid structure coupling analysis was executed.

2.2. FlowVision Air Pumping Noise Model

Fig. 5 depicts the domain size and the initial grid of air. If the domain size was too small, the boundary will affect the flow field near the tire. After testing several domain sizes, the size of 2.4 × 1.4 × 1.5 m was deemed appropriate.

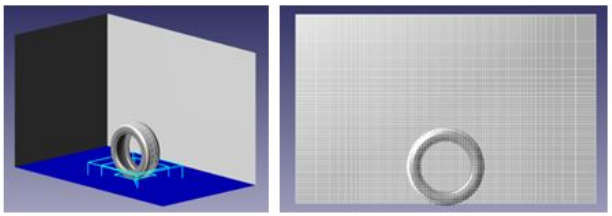

Fig. 5. FlowVision air pumping noise model and the mesh of the domain.

The boundary conditions of the six surfaces of the domain were defined as symmetry. Air property uses FlowVision's built-in data (Air_Gas), and air is defined as a Newtonian fluid. The initial velocity of the flow field was zero.

The initial size of the mesh is smaller near the tire and bigger near the domain boundaries, and FlowVision's local refinement function was used to refine the mesh. Fig. 6 depicts the mesh refinement in three levels. The area which was closest to the bottom of the tire was refined with level 3, which means that a grid was divided into 64 grids in the two-dimensional mesh. The next area was refined with level 1 and 2. In addition, the area near the surface of the tread was defined as 5 cell strata and had a refinement of level 1. It means that there are 5 grids that are refined with level 1 as we move outward from the tread surface.

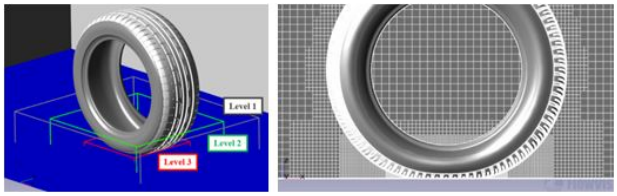

Fig. 6. Refinement of mesh in three levels.

Fig. 7 depicts the velocity distribution of the flow field. If it has enough distance between the tire and air domain boundary, the flow field around the tire is not affected by the air domain boundary, and the best results can be obtained with local refinement. Fig. 8 shows the area that records the change in sound pressure. After the sound pressure change was obtained, we can calculate the total sound pressure level and spectrum for further study.

2.3. Material Properties

2.3.1. Hyperelasticity

Rubber is a hyperelastic material. The relationship of rubber's stress-strain curve is nonlinear, and it remains elastic even after large deformations. Therefore, the material behavior of rubber cannot be defined with linear relationships. It must use the change of strain energy to describe

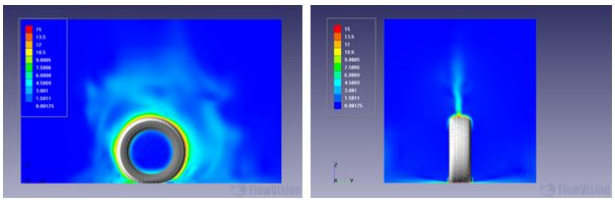

Fig. 7. Velocity distribution of the flow field.

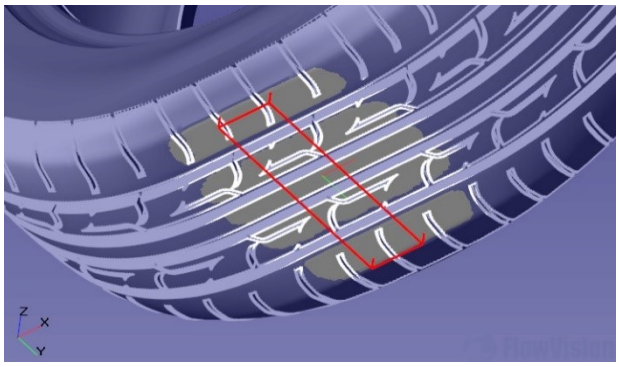

Fig. 8. Detailed area that records the sound pressure change.

the deformation. The behavior of hyperelasticity can be described by a strain energy function, such as those of Marlow, Oden, Mooney-Rivlin, and Yeoh. This study utilizes the Marlow model [10] to define the material behavior of rubber. Equation (1) [11] defines the Marlow model:

$$U = U_{dev}(\overline{I_1}) + U_{vol}(J_{el}) \tag{1}$$

where the first term is defined from the tensile test data, and the second is defined from Poisson's ratio. Fig. 9 illustrates the result of the test data and Marlow fitting. After obtaining the coefficients of strain energy function through fitting curve, we can differentiate the function to describe the change of material stiffness and stress for an element during rubber deformation.

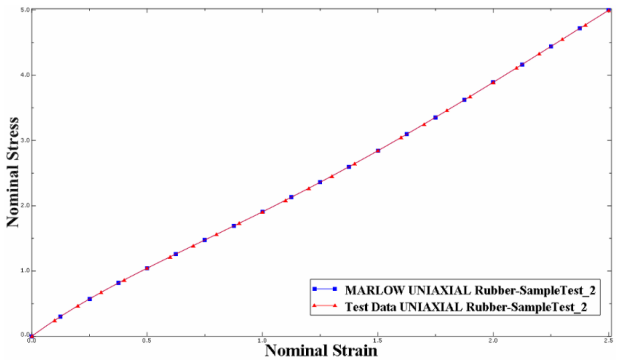

Fig. 9. The result of the test data and Marlow fitting.

2.3.2. Belt, Belt cover, and Ply

In addition to rubber, tire contains nylon, and steel wire. The diameter, density, and angle of the nylon and steel wire are different according to the requirements of performance. The size of the fiber is significantly smaller than the whole tire. If we use the continuum elements to establish the fiber, it is difficult to build the model, and the related calculation takes a lot of time. Therefore, the fiber layers of the tire, such as the belt, belt cover, and ply, were defined by the rebar layer [11]. When we establish the 2-D axisymmetric model, each fiber layer uses the SFMGAX1 element. The rebar layer parameters to be considered are the cross-sectional area, the distance between the fibers, and the angle of the local coordinate of the element.

2.4. Calculation of Noise

Fig. 10 illustrates the process of noise calculation. After the fluid structure coupling was simulated by Abaqus's tire model and FlowVision's air pumping noise model, the change of sound pressure over time is obtained from FEM model. Then, using fast Fourier transforms, the time domain of sound pressure p(t) can be converted to the frequency domain of sound pressure p(f). The human ear's feeling of sound change is a log relationship, and the lowest sound pressure that human ears can basically feel is 2×10^{-5}Pa. We use the Equation (2) to convert the sound pressure p(f) to decibels, and observe the decibel value corresponding to each frequency.

$$L_p = 20\log\frac{p_{rms}}{p_0} \tag{2}$$

where p_{rms} is the effective sound pressure and p_0 is the reference sound pressure. The reference sound pressure is $2 \times 10^{-5} Pa$. Because the human ear feels different at different frequencies, it needs to add A-weighting to the model. After adding A-weighting, the form of data was the same as the spectrum obtained from the experiment. The total sound pressure level was calculated by adding the sound pressure level of each frequency. This study used the spectrum and total sound pressure level to discuss and verify the effectiveness of the proposed model.

3. Results

3.1. Experimental Data and Verification

The indoor test was executed at ARTC (Automotive Research & Testing Center). Fig. 11 depicts the three tires used for testing. The air pumping noise model for tires was established for each tire. The tread pattern was based on the design of tire groove that added the lateral groove and small tread pattern.

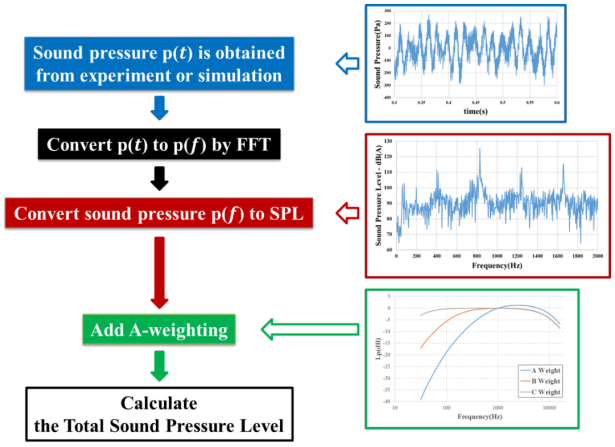

Fig. 10. The process of noise calculation.

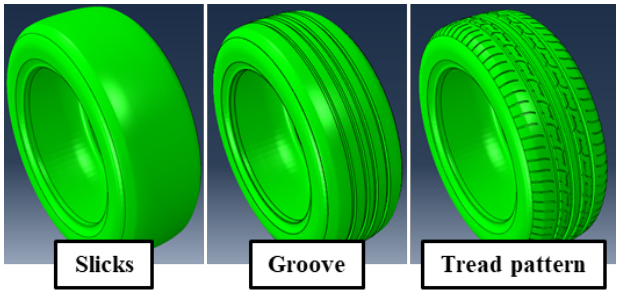

Fig. 11. The type of tread pattern.

The test conditions were defined as an inflation pressure of 180 kPa, load of 475 kgf, velocity of 30–100 km/h, frequency range of 22.4–3200 Hz and a frequency resolution of 4 Hz. The microphone was installed at a distance of 50 cm from the center of the tire and 25 cm from the ground.

Fig. 12 depicts the noise of the three tires at different speeds. The noise of the tread pattern was the largest, and the slicks and groove have special results. When the velocity was less than 70 km/h, the noise of the groove was higher than the slicks. However, the noise of the slicks and groove was almost the same when the velocity was higher than 70 km/h. It can be seen that the noise of the slicks and groove was not much different at speeds of 80 and 100 km/h. The spectrum was further utilized to study why the noises of the slicks and groove were almost the same.

Fig. 13 shows the noise spectra for slicks, groove and tread patterns at speeds of 40, 60, 80 and 100 km/h. There is a peak at a frequency of 400–600 Hz for slicks and groove tires, and it is generated by the carcass vibration and inner standing wave. Next, the spectra of the groove tire were discussed. Around 1200 Hz, the highest peak observed is for the groove tire during compressing and releasing air. The noise caused by groove is significantly louder than

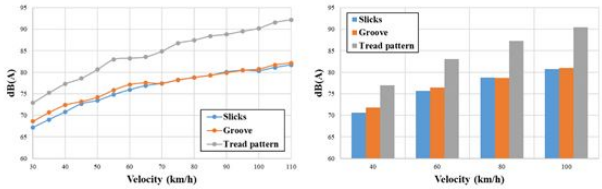

Fig. 12. The noise of different tread patterns at different velocities.

the noise caused by carcass vibration and inner standing wave. If we see the change of peak around 1200 Hz at different velocities, the noise generated by the groove increases when the velocity is increased from 40 to 60 km/h. However, the change is less when the speed was higher than 60 km/h, but the noise at low frequency (400–600 Hz) continues to increase. The same relationship was observed for the slicks. Therefore, after the speed increases to more than 60 km/h, the increasing noise is caused by carcass vibration and inner standing wave.

In comparing the groove and tread pattern, the peak and frequency of noise of the tread pattern were different for changing velocities because the tread pattern has a complex design, such as lateral grooves, small tread patterns, and pitch arrangements. It was seen that when the velocity increases, the noise also increases. This means that the influence of tread pattern on noise is greater than that of the carcass vibration and inner standing wave. Therefore, the noise source of slicks is carcass vibration and inner standing wave, and the noise source of the groove tires is the groove design, when the speed is less than 60 km/h. The tread pattern produces louder noise than carcass vibration, inner standing wave, and groove design.

The noise spectra comparing the simulation results with the experimental data of the slicks, groove and tread pattern are illustrated in Figs. 14-16.

Fig. 14 shows that the simulation of noise of slicks is zero. It is reasonable because the model simulates the air pumping noise generated by tread pattern and the sound pressure is captured in the area of Fig. 8. There is no pattern design on slicks and, therefore, air is not compressed and released to generate noise.

Fig. 15 shows the noise spectrum of the groove. The maximum value of the experimental data is close to 70 dB, while the simulation results show ∼120 dB. The difference between the experimental data and simulation is the location recording the sound pressure change. The experimental data records the sound pressure change at a distance from the tire, but the simulation obtains the sound pressure from the bottom of the tire. Therefore, the noise of

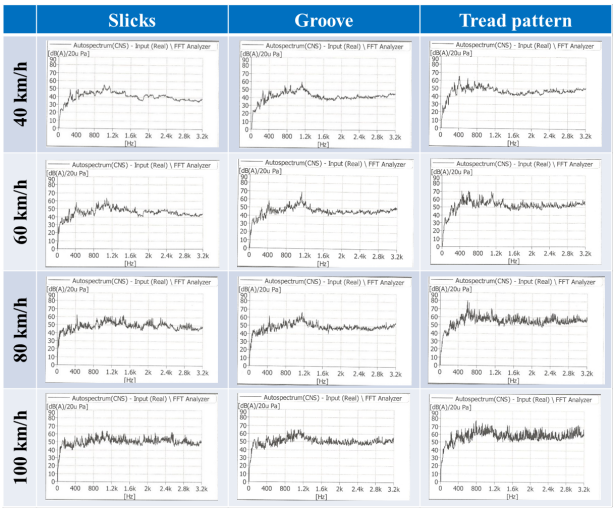

Fig. 13. The noise spectra of different tread patterns at different velocities.

simulation is relatively large. If the transmission of sound is taken into account in simulation, the increased domain causes the computational time to increase, and the very small change of sound pressure may not be calculated by FlowVision. Hence, we combined the simulation results and experimental data to discuss the trend of the change and peak. It is observed that there is a peak around 1200 Hz regardless of the experiment or simulation. It means that the model can accurately simulate the noise generated by groove due to air pumping. The experimental data has the peak of 400 Hz generated by carcass vibration and inner standing wave, but the simulation result does not show this peak. As the model only simulates the air pumping effect, it is reasonable to observe that there is no peak near 400 Hz in the simulation results.

Fig. 16 depicts the spectrum of the tread pattern. The peaks at 1200 Hz still exist because the tread pattern includes the groove design. Whether it is the simulation results or experimental data, there is a peak at 600 Hz, which is greater than the peak at 1200 Hz. This peak was generated by lateral groove, small tread pattern, and pitch arrangement.

By comparing the simulation results with the experimental data, it can be seen that the model accurately simulates the noise generated by the air pumping effect. The model can be utilized to study the influence of tread pattern design on the frequency distribution and the value of the peak. This paper utilizes this model to study the pitch arrangement of the tread pattern.

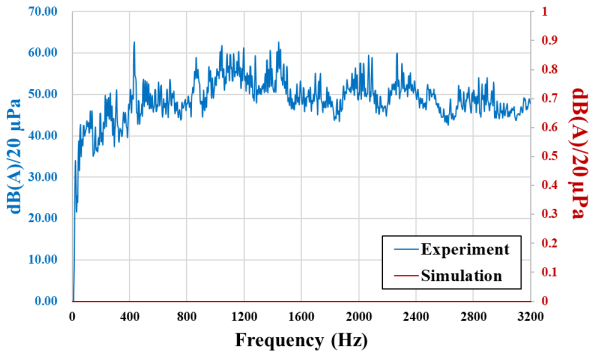

Fig. 14. Comparison of the simulation results and experimental data for slicks.

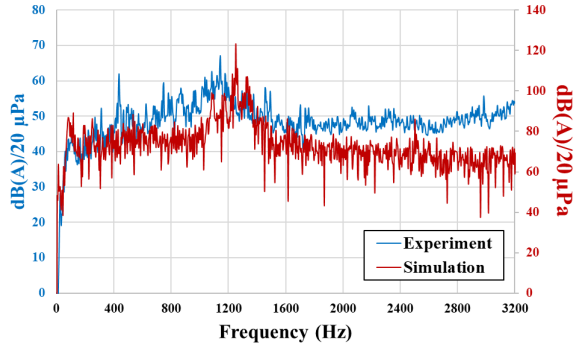

Fig. 15. Comparison of the simulation results and experimental data for groove.

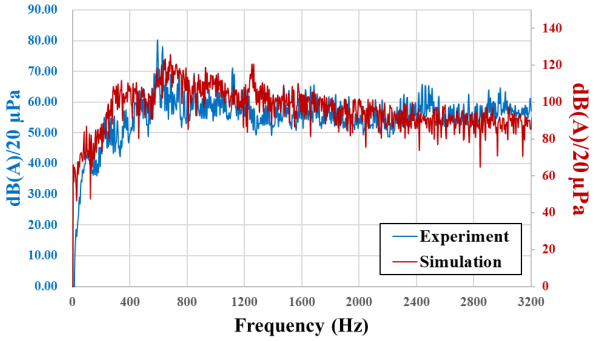

Fig. 16. Comparison of the simulation results and experimental data for tread pattern.

3.2. Pitch Arrangement

The study of pitch arrangement was based on the tread pattern design of Fig. 11. Fig. 17 depicts the pitch arrangement of the original design. The numbers of pitch A, B, and C were 12, 7, and 11, and the lengths were in the order pitch A > pitch B > pitch C.

Fig. 18 depicts the single pitch arrangement that con-

sisted of 36 pitch C. Fig. 19 shows the simulation results of the original design and single pitch design. There was a difference in frequency distribution. The frequency peaks for the single pitch were at 400, 800, 1200, and 1600 Hz. If one assumes a velocity of 80 km/h and a tire radius of 312.5 mm, the tire rolls 11.32 revolutions per second. The first frequency can be calculated as $f_1 = 11.32 \times 36 = 407.64$ Hz, the second frequency $f_2 = 407.64 \times 2 = 815.28$ Hz, and the third frequency $f_3 = 407.64 \times 3 = 1222.92$ Hz. The results of the mathematical calculations were consistent with the peaks in the frequency distribution. It can be seen that the number of pitches has a direct influence on the frequency distribution of noise. If a single pitch was used, the noise was very loud. Using different pitch lengths and arrangements can effectively reduce noise.

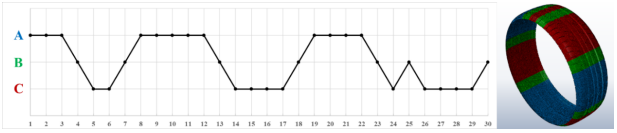

Fig. 17. Pitch arrangement of the original design.

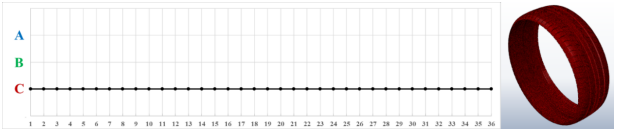

Fig. 18. The single pitch arrangement.

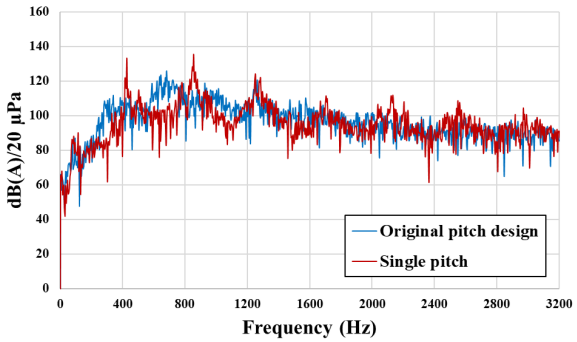

Fig. 19. Comparison of the original pitch design and single pitch arrangement.

Figs. 20 and 22 depict the different pitch arrangements, pitch design 1 and 2. The two designs use the same number of pitch A, B, and C as in the original design. Pitch design 1 divides one of the segments of pitch A into more pieces, and pitch design 2 divides most of pitch A and C into more pieces. Figs. 21 and 23 show the results of the two designs and compare with the original pitch design. The sound pressure (unit: Pa) is presented for each figure to observe the differences in the peaks.

The frequency distribution is similar between the two designs and original design because the number of pitches was the same. The total sound pressure of the original pitch design was 137.256 dB(A), pitch design 1 was 137.292 dB(A) and pitch design 2 was 137.017 dB(A). The sound pressure level was converted to sound pressure to compare each pitch design since the spectra of sound pressure level are difficult to distinguish.

In comparing pitch design 1 and the original design, there is a peak near 600 Hz. The maximum peak of 600 Hz can be reduced when using pitch design 1. However, there are more peaks generated around 600 Hz. Although each peak is smaller than the peak of the original design, the total sound pressure level was increased. The difference between sound of the two designs was about 0.04 dB.

The difference between the maximum peak for design 2 and the original pitch is less than that for the pitch of design 1 and the original pitch. However, it can effectively reduce the peaks around the maximum peak. Therefore, the total sound pressure level can be reduced by about 0.25 dB, which is an improvement in sound reduction.

Based on the simulation results, it is better to reduce noise if the pitch arrangement is dispersed as in pitch design 2. In this design, the frequency distribution will not be affected if the number of each pitch is not changed. It also shows that changing the pitch arrangement will mainly affect the peak of the sound pressure. Hence, the number of pitches must be altered if the frequency distribution is changed.

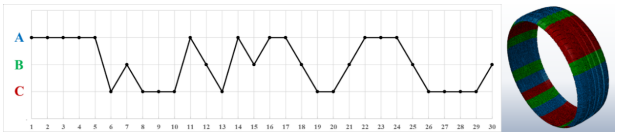

Fig. 20. Pitch design 1.

Finally, the tread pattern is changed to a snow tire type to discuss the influence on noise, with a tire size of 205/55R16 94H. Figs. 24 and 25 depict the pitch arrangements of two designs, where the number of pitch A, B, and C are the same. Pitch 1 is a dispersed design, and pitch 2 is a periodic design. Fig. 26 is the spectra of the simulation results. It can be seen that the frequency distribution is very close because the number of pitches of the two designs is the same. Two designs have a maximum peak around 600 Hz, and the peak of pitch design 1 was lower than pitch design 2. The total sound pressure level of pitch design

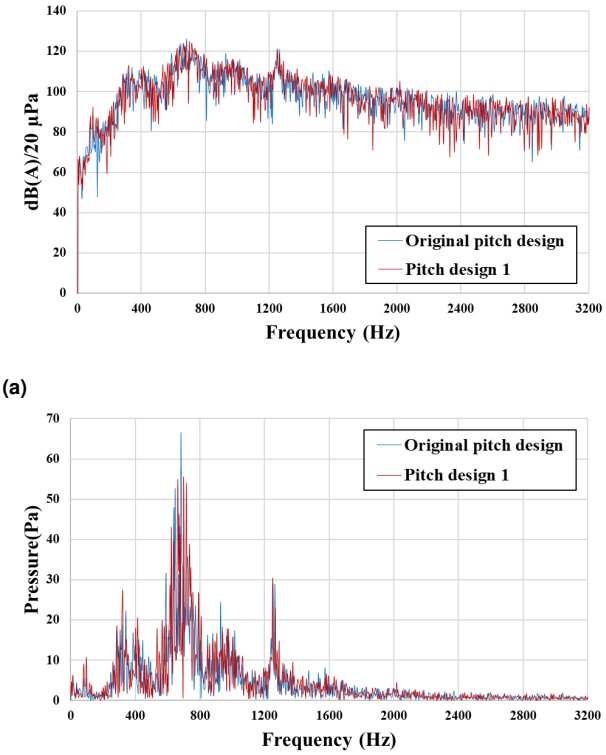

Fig. 21. Spectra for pitch design 1: (a) sound pressure level of the pitch design, and (b) sound pressure of the pitch design.

Fig. 22. Pitch design 2.

1 and pitch design 2 are 142.62 dB and 143.52 dB, respectively. It can be seen that it is effective to reduce noise if the pitch arrangement is dispersed to avoid the periodic arrangement, regardless of the type of tread pattern.

4. Conclusions

This study establishes an air pumping noise model for tires that simulates fluid structure coupling and obtains the change in sound pressure to calculate noise. The model was verified using experimental data, and the trends of the peak and frequency distribution match the experimental data very well. The order of calculated noise was higher than the experimental data because the model obtains the sound pressure at the bottom of tire. However, the model can be utilized to study the influence of air pumping and

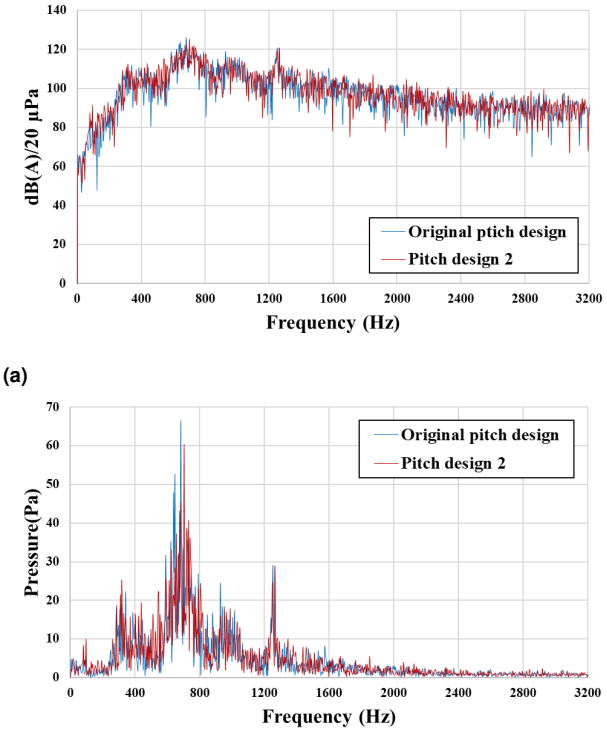

Fig. 23. Spectra for pitch design 2: (a) sound pressure level of the pitch design, and (b) sound pressure of the pitch design.

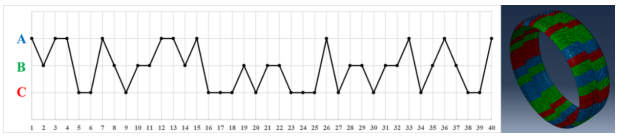

Fig. 24. Snow tire - pitch design 1.

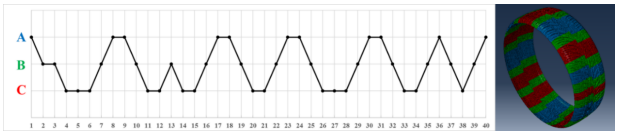

Fig. 25. Snow tire - pitch design 2.

tread pattern design on noise.

In case of pitch arrangement, if the single pitch arrangement and varying numbers of pitches are used, the frequency distribution is very different. It can be seen that the number of pitches has a direct influence on noise and frequency distribution. If the number of pitches is same, the frequency distribution of the peak does not change when the pitch arrangement is modified. It also verifies that the frequency distribution is related to the number of pitches and changing the arrangement mostly affects the peak of

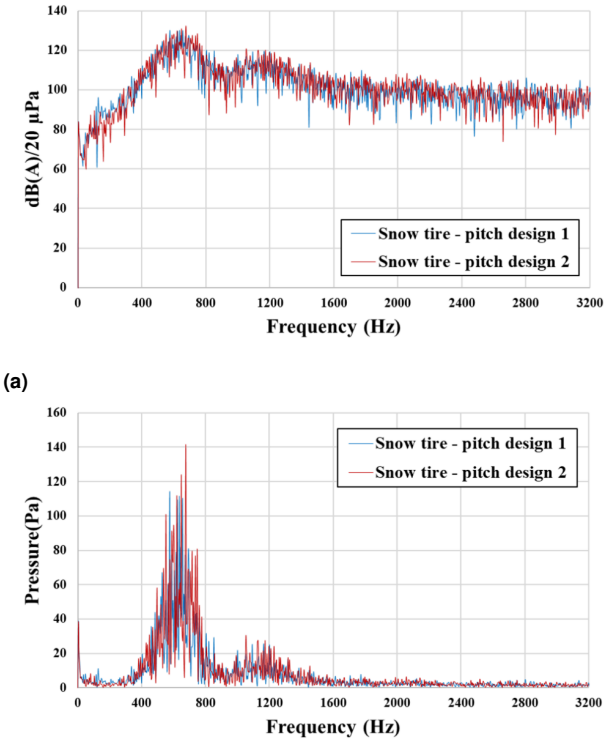

Fig. 26. Spectrum of a snow tire: (a) sound pressure levels of the pitch designs, and (b) sound pressures of the pitch designs.

the sound pressure. From the analysis, if pitch arrangement is dispersed more to avoid the periodic arrangement, it can effectively reduce noise regardless of the type of tread pattern.

The air pumping noise model for tires can continue to be develop further in the future, such as considering more complex interactions with other factors, or using the result as input for sound transmission analysis. The more factors can be studied and obtain more insight.

5. Acknowledgements

The authors acknowledge the NANKANG Rubber Tire Corporation, Ltd. for the financial and technical supports of this study.

References

[1] UNECE. UNECE Regulation No. 117 - Uniform provisions concerning the approval of tyres with regard to rolling sound emissions and/or to adhesion on wet surfaces and/or to rolling resistance.

[2] M.-X. Huang and R.-J. Shyu. Study of Tire Noise Generation Mechanism,. *The 36th National Conference on Theoretical and Applied Mechanics, Taoyuan, R.O.C*, 2012.

[3] Y.-H. Huang. Studies of Noise Reduction with Designs of Tire Tread Patterns. Master's thesis, National Taiwan University, R.O.C., 2016.

[4] T. Sakata, H. Morimura, and H. Ide. Effects of tire cavity resonance on vehicle road noise. *Tire Science and Technology*, 18(2):68–79, 1990.

[5] H. M. R. Aboutorabi and L. Kung. Application of coupled structural acoustic analysis and sensitivity calculations to a tire noise problem. *Tire Science and Technology*, 40(1):25–41, 2012.

[6] S. Fujiwara, K. Yumii, T. Saguchi, and K. Kato. Reduction of tire groove noise using slot resonators. *Tire Science and Technology*, 37(3):207–223, 2009.

[7] Y. Wei, X. Feng, Z. Fuqiang, and D. Xiang. Simulation of Rolling Noise Based on the Mixed Lagrangian–Eulerian Method. *Tire Science and Technology*, 44(1):36–50, 2016.

[8] M.-X. Huang and J.-Z. Tu. Study of Tread Pattern Noise, 2009.

[9] FlowVision Users guide Verson 3.09.05. .

[10] R. S. Marlow. A general first-invariant hyperelastic constitutive model. *Constitutive Models for Rubber*, pages 157–160, 2003.

[11] ABAQUS Analysis User's Manual. .